

Liquid-Liquid Critical Point in 3D Many-Body Water Model

Luis Enrique Coronas,¹ Valentino Bianco,¹ Arne Zantop,² and Giancarlo Franzese^{1,*}

¹*Facultat de Física, Universitat de Barcelona, Diagonal 645, 08028 Barcelona, Spain.*

²*Max Planck Institute for Dynamics and Self-Organization, Am Fassberg 17, 37077 Göttingen, Germany*

(Dated: August 29, 2018)

Many-body interactions can play a relevant role in water properties. Here we study by Monte Carlo simulations a coarse-grained model for bulk water that includes many-body interactions associated to water cooperativity. The model is efficient and allows us to equilibrate water at extreme low temperatures in a wide range of pressures. We find the line of temperatures of maximum density at constant pressure and, at low temperature and high pressure, a phase transition between high-density liquid and low-density liquid phases. The liquid-liquid phase transition ends in a critical point. In the supercritical liquid region we find for each thermodynamic response function a locus of weak maxima at high temperature and a locus of strong maxima at low temperature, with both loci converging at the liquid-liquid critical point where they diverge. Comparing our results with previous works for the phase diagram of a many-body water monolayer, we observe that the weak maxima of the specific heat are less evident in bulk and appear only at negative pressures, while we find those of compressibility and thermal expansion coefficient also at positive pressures in bulk. However, the strong maxima of compressibility and thermal expansion coefficient are very sharp for the bulk case. Our results clarify fundamental properties of bulk water, possibly difficult to detect with atomistic models not accounting for many-body interactions.

I. INTRODUCTION

Water models are of fundamental importance in many fields of physics, chemistry, biology and engineering. For example, it is now commonly accepted that water plays a key role in protein folding [1–6] and protein dynamics [7–12]. Computer simulations are an important tool to study such phenomena. Nevertheless, the computational cost for full-atom simulations of large-scale biological systems with explicit water for experimentally-relevant time-scales is often prohibitive. Therefore, it is necessary to explore alternative approaches that could allow us to access mesoscopic scales and time-scales of the order of seconds. A possible solution is to develop coarse-grain models of water that could greatly reduce the simulation cost for the solvent preserving its main physical properties.

Despite the importance of water in many aspects of life, there are still open questions concerning its complex nature. Water exhibits more than 60 anomalies [13], like the existence of a density maximum in the liquid phase at ambient pressure and temperature $T \sim 4^\circ\text{C}$ or the anomalous increase of the specific heat C_P , isothermal compressibility K_T , and absolute value of the thermal expansivity α_P upon cooling liquid water toward the melting line and below it, in the supercooled liquid state [14]. A common understanding is that all these peculiar properties of water are related to its hydrogen bonds (HBs) forming a network that orders following tetrahedral patterns at low T [15]. A large number of classical atomistic water models have been proposed in the last decades with some performing better than others [16].

Nevertheless, there is still no atomistic model able to fit all the water properties [16]. One possible reason for it is that pair-additive potentials do not capture the effective many-body interactions due to quantum effects and polarizability [17–20]. Consistent with this view, the effect of these many-body interactions are stronger where the water anomalies are more evident [21].

The origin of anomalous properties of water has been largely debated since the 80's [22–43] and a series of thermodynamic scenarios have been proposed [44–47]. In particular, Poole et al., based on molecular dynamic simulations, proposed a liquid-liquid second critical point (LLCP) in the supercooled region [46]. According to this scenario, the LLCP is located at the end of a first order phase transition separating two liquid metastable phases of water with different density, structure and energy [35, 39, 42]. Extrapolations from experimental data [48], based on the hypothesis of such a critical point, show that the maxima in response functions should be much stronger and at lower temperature than those predicted by the classical model used in Ref. [46]. However, equilibrate classical models at very low T is extremely computationally demanding, making difficult to settle the disagreement between the simulations and the extrapolated experimental data.

We propose a coarse grained (CG) bulk water model that includes many-body interactions in a computationally effective way. Our results extend those for a previous model of a many-body water monolayer, able to reproduce the main features of water in a very efficient way and at those extreme conditions that are not easily reachable by atomistic simulations [35, 49–53]. Here we show that the bulk model exhibits a liquid-liquid phase transition (LLPT) in the supercooled region, as the monolayer. We find a relevant difference between the results for the response functions in the the bulk model and those in the

* gfranzese@ub.edu

monolayer. In both cases we observe a line of weak maxima and a line of strong maxima for the response functions in the pressure-temperature phase diagram, however the C_P weak maxima in bulk water are observable only at negative pressure, at variance with the monolayer case.

The paper is organized as follows. In Section II we define the coarse-grain model for bulk water with effective many-body interactions. In Section III we describe the simulation method. In Section IV we present and discuss our results. In Section V we give our conclusions. In Appendix A we present further details of the phase diagram and in Appendix B we explain the details of the equilibration and the error calculations.

II. THE MANY-BODY WATER MODEL

We consider a system of a constant number of molecules N , pressure P and temperature T in a variable volume V . We partition the total volume V into a regular cubic lattice of \mathcal{N} cells, $i \in [1, \dots, \mathcal{N}]$, each with volume $v_i \equiv V/\mathcal{N}$. For sake of simplicity we set $\mathcal{N} = N$ and consider the case of a homogeneous fluid, in such a way that each cell is occupied by one water molecule. Next we introduce a discretized density field $n_i \equiv \theta(2 - v_i/v_0)$, where the Heaviside step function $\theta(x)$ is 0 or 1 depending if $x < 0$ or ≥ 0 , corresponding to gas-like or liquid-like local density, respectively, and $v_0 \equiv 4/3\pi(r_0/2)^3$ is the van der Waals volume of a water molecules, with $r_0 \equiv 2.9$ Å.

The Hamiltonian of the system is by definition the sum of three terms

$$\mathcal{H} \equiv \mathcal{H}_{\text{vdW}} + \mathcal{H}_{\text{HB}} + \mathcal{H}_{\text{coop}}, \quad (1)$$

corresponding to the van der Waals isotropic interaction, the directional and the cooperative contribution to the HB interaction, respectively. A detailed description and motivation for each term can be found in Ref.s [35, 51, 53].

The van der Waals Term is given by the sum over the contributions of all pairs of molecules i and j ,

$$\mathcal{H}_{\text{vdW}} \equiv \sum_{\langle i,j \rangle} U(r_{ij}), \quad (2)$$

where $U(r)$ is a Lennard-Jones potential with a hard-core (van der Waals) diameter r_0 , i.e.

$$U(r) \equiv \begin{cases} \infty & \text{if } r \leq r_0 \\ \epsilon \left[\left(\frac{r_0}{r}\right)^{12} - \left(\frac{r_0}{r}\right)^6 \right] & \text{if } r_0 > r > r_c \\ 0 & \text{if } r_c < r. \end{cases} \quad (3)$$

We truncate the interaction at a distance $r_c \equiv 6r_0$.

The second terms in Eq. (1) is defined as

$$\mathcal{H}_{\text{HB}} \equiv -JN_{\text{HB}} \equiv -J \sum_{\langle i,j \rangle} n_i n_j \delta_{\sigma_{ij} \sigma_{ji}} \quad (4)$$

where N_{HB} is the total number of HB in the system. A water molecule i can form up to four HBs with molecules j at a distance such that $n_i n_j = 1$, i.e. $v_i \leq 2v_0$ implying a water-water distance $r_{i,j} \leq 2^{1/3}r_0 \simeq 3.7$ Å. Furthermore, to form a HB the relative orientation of the two water molecules must be such that the angle between the OH of a molecules and the O-O direction does not exceed $\pm 30^\circ$. Hence, only 1/6 of the entire range of values $[0, 360^\circ]$ for this angle is associated to a bonding state. We account for this constrain introducing a bonding variable $\sigma_{ij} \in [1, q]$ of molecule i with each of the six nearest molecules j and setting $q = 6$ to account correctly for i) the contribution to the HB energy via the $\delta_{\sigma_{ij} \sigma_{ji}} \equiv 1$ if $\sigma_{ij} = \sigma_{ji}$, 0 otherwise, and ii) the entropy variation due to the HB formation and breaking. We set $J/4\epsilon = 0.5$, consistent with the proportion between the van der Waals interaction and the directional (covalent) part of the HB interaction.

The last term in the Hamiltonian accounts for the cooperativity of the HBs and is an effective many-body interaction between HBs due the O-O-O correlation that locally leads the molecules toward an ordered (tetrahedral) configuration

$$\mathcal{H}_{\text{coop}} \equiv -J_\sigma N_{\text{coop}} \equiv -J_\sigma \sum_i n_i \sum_{\langle kl \rangle_i} \delta_{\sigma_{ik} \sigma_{il}}, \quad (5)$$

where the sum is over the six bonding indices of the molecules i with the molecules k and l , both near i . By setting $J_\sigma/4\epsilon = 0.03$, with $J_\sigma \ll J$, we guarantee that this term is relevant only at those temperatures below which the molecule i has already formed (non-tetrahedral) HBs with the molecules k and l , implying an effective many-body interaction of molecule i with the four bounded molecules in its hydration shell.

A consequence of the formation of a network of tetrahedral HBs is the increase of proper volume associated to each molecule. The model takes this effect into account on average by adding a small increase of volume $v_{\text{HB}} = 0.5v_0$ per bond, consistent with the average volume increase between high- ρ ices VI and VIII and low- ρ (tetrahedral) ice Ih. Therefore, the total volume of the system with N_{HB} HBs is

$$V \equiv Nv_0 + N_{\text{HB}}v_{\text{HB}}. \quad (6)$$

The tetrahedral local rearrangement does not change the average water-water distance, therefore the distance r in Eq.(3) is not affected by the change in Eq.(6).

The enthalpy H of the model is therefore

$$H \equiv \sum_{\langle i,j \rangle} U(r_{ij}) + JN_{\text{HB}} + J_\sigma N_{\text{coop}} + PV \quad (7)$$

and the volume contribution to the entropy is

$$S_V \equiv -k_B \ln(V/v_0). \quad (8)$$

The model presented here by definition does not include crystal phases, i.e. at any T and P our course

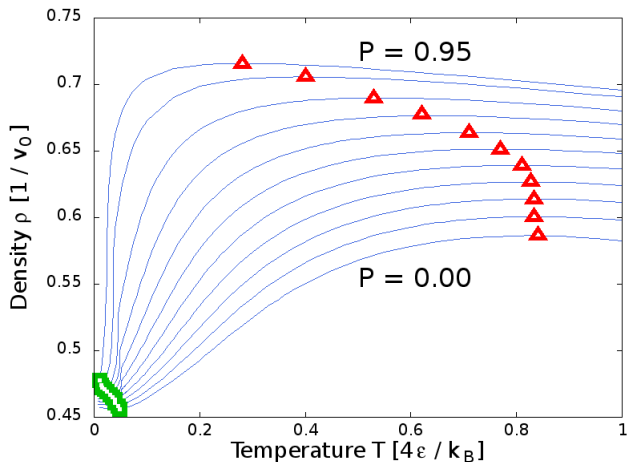


FIG. 1. Density along isobars for (from bottom to top) $Pv_0/(4\epsilon) = 0.00, 0.10, 0.20, 0.30, 0.40, 0.50, 0.60, 0.70, 0.80, 0.90, 0.95$. At each P we find a temperature of maximum density, TMD (red triangles) and a temperature of minimum density, TminD (green squares). For sake of clarity we show the interpolated equation of state and do not show the calculated state points.

grain water can be equilibrated in its fluid state after a large enough equilibration time. Furthermore in our coarse graining we neglect water translational diffusion, focusing only on the local rotational dynamics of the HBs. Formulation of the model that include translation diffusion and crystal polymorphism can be found in Ref. [53] and Ref. [54], respectively, for the monolayer case. Analogous formulations can be introduced also for the bulk model. It's worth noting, however, that the present definition includes structural and densities heterogeneities associated to the HB network dynamics.

III. SIMULATION METHOD

We perform Monte Carlo (MC) simulations at constant $N = 8000$, constant P and constant T in a cubic (variable) volume V with periodic boundary conditions along two axis [55]. We update the HB network with the Wolff Monte Carlo (MC) cluster algorithm adapted to the present model, as explained in Ref. [56].

We calculate the equation of state along isobars in the range of $Pv_0/(4\epsilon) \in [-0.5, 0.95]$ separated by intervals of $\Delta P \leq 0.05(4\epsilon)/v_0$. The range of temperatures is $Tk_B/(4\epsilon) \in [0.02, 1.0]$ with $\Delta T \geq 0.01(4\epsilon)/k_B$ if $Tk_B/(4\epsilon) \in (0.1, 1.0]$, and $\Delta T \geq 0.001(4\epsilon)/k_B$, if $Tk_B/(4\epsilon) \in [0.02, 0.1]$. We calculate each isobar by sequential annealing starting at $T = 7(4\epsilon)/k_B$ and letting the system equilibrate, as explained in details in Appendix A. For each state point we average over 10^6 MC steps after equilibration, with a number of independent configurations between $10^2 - 10^3$ depending on the state point.

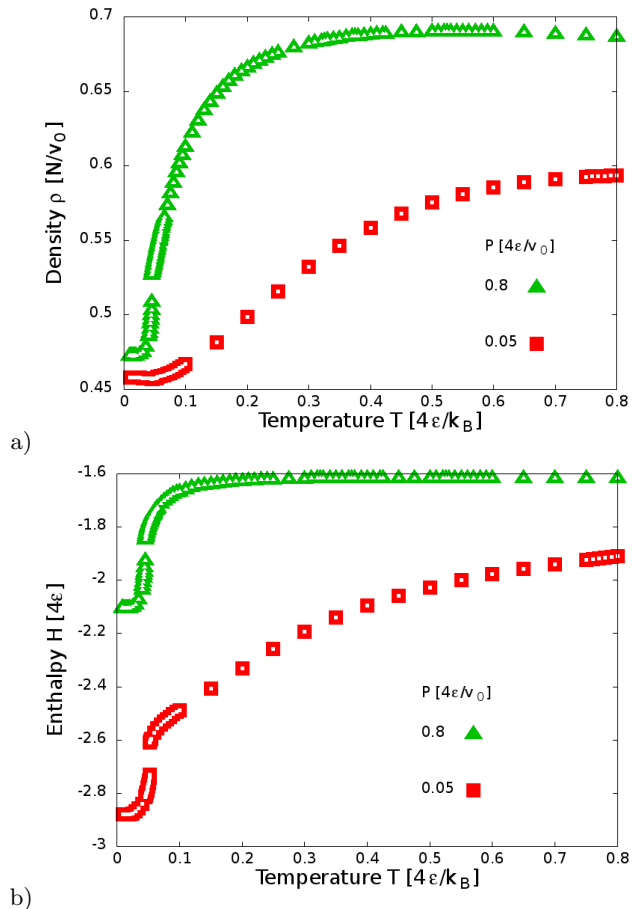


FIG. 2. a) Isobaric variation of density and b) enthalpy as a function of temperature for high pressure ($Pv_0/(4\epsilon) = 0.80$, green triangles) and low pressure ($Pv_0/(4\epsilon) = 0.05$, red squares).

IV. RESULTS AND DISCUSSION

At temperatures below the gas-liquid phase transition (Appendix A), we find along isobars a temperature of maximum density (TMD) (Fig. 1) as in water. By further decreasing T , we observe a sharp decrease of the isobaric density $\rho \equiv N/V$ and a temperature of minimum density TminD (Fig. 1). This behavior is consistent with the LLPT between a high density liquid (HDL) and a low density liquid (LDL) as postulated for supercooled liquid water [46]. However, a similar behavior, but without any discontinuity, is predicted also by the “singularity free” scenario [30, 45, 57]. We therefore analyze the enthalpy behavior in detail.

We find that H follows the density but with sharper changes at any P (Fig. 2). At high P both density and enthalpy display a seemingly discontinuous change, while for low P the variation in density becomes much smoother than the enthalpy change.

We understand the behavior of ρ as a consequence of its dependence on N_{HB} from Eq.(6). A direct calculation shows that by decreasing T the model displays a rapid

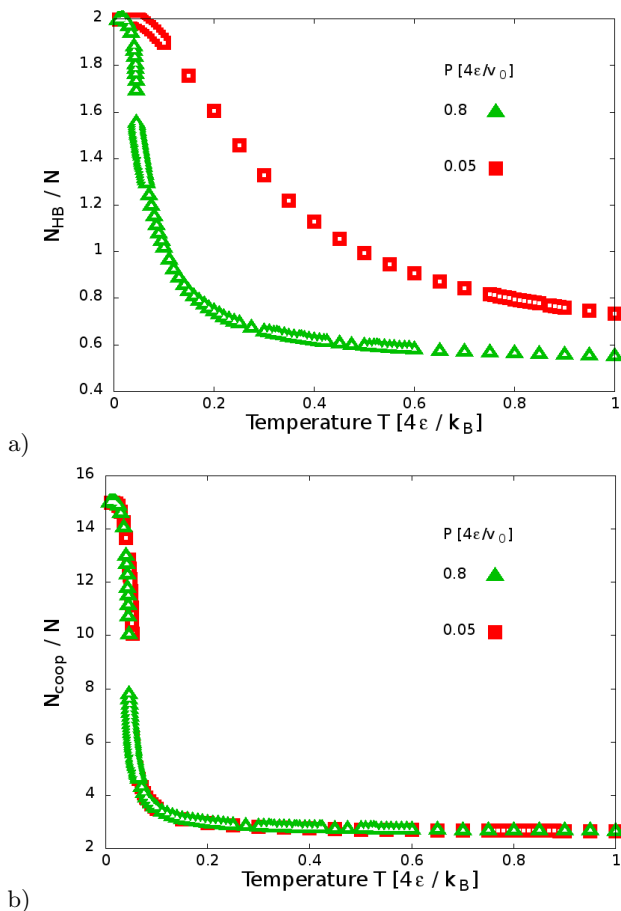


FIG. 3. a) Isobaric variation of the number of HB per molecule N_{HB}/N and b) the number of cooperative bonds per molecule N_{coop}/N . While N_{HB} strongly depend on P , N_{coop} is almost P -independent.

increase of N_{HB} at high P , while the increase is progressive at low P (Fig. 3a). In particular, we find that N_{HB} saturates at low T to two HBs per molecule, corresponding to the case where every water molecule is involved in four HBs. At high T the number N_{HB}/N is $\simeq 1/2$ at high P and is $\simeq 0.7$ at low P , with each molecule forming on average one HB or less than two, respectively.

Nevertheless, the changes of N_{HB} are never discontinuous as in the enthalpy, clearly showing that the contribution to H coming from the other terms in Eq.(7) are relevant. The explicit calculation of these terms shows that the dominant contribution comes from the behavior of N_{coop} (Fig. 3b). We find that N_{coop} has a sharp, but continuous, increase at any P within the range investigated. Furthermore, at variance with what observed for N_{HB} , the temperature of the largest increase of N_{coop} is almost independent on P . This temperature coincides with the largest variation of H at any P and with the large change of ρ at high P . Therefore, the largest variation of H is associated with the cooperative contribution that, in turns, is a consequence of a large structural rear-

range of the HBs toward a more tetrahedral configuration. However, at low P this reorganization of the HBs occurs when the number N_{HB} of HBs is almost saturated, implying only a minor change in ρ . On the other hand, at high P the restructuring of the HBs occurs at the same time as the formation of a large amount of them, up to saturation. Therefore, the effect on the density is large and collective, as expected at a critical phase transition.

A further way to clarify if the observed thermodynamic behavior is consistent with the occurrence of a LLPT ending in a critical point is to calculate the response functions C_P , K_T and α_P and to study if they diverge at the hypothesized LLCP. At equilibrium all these quantities correspond to thermodynamic fluctuations. Therefore, we calculate the specific heat along isobars both by numerical derivative of H , $C_P \equiv (\partial\langle H \rangle / \partial T)_P$, and by the fluctuation-dissipation theorem $C_P = \langle H^2 \rangle / k_B T^2$. In this way we reach a better estimate of C_P and at the same time, by verifying the validity of fluctuation-dissipation theorem, we guarantee that the system is equilibrated (Appendix B).

We find strong maxima in C_P at any P and low T . For $Pv_0/(4\epsilon) \leq 0.85$ the maxima occur all at the same T and increase as the pressure increases with an apparent divergence of C_P at $Pv_0/(4\epsilon) = 0.85$ (inset Fig. 4a). However, for $Pv_0/(4\epsilon) > 0.85$ the maxima decrease in intensity and moves toward lower T (Fig. 4a). This behavior is consistent with a LLCP occurring at $Pv_0/(4\epsilon) \simeq 0.85$ at the end of a first-order phase transition occurring at higher P along a line with a negative slope in the P - T thermodynamic plane, as expected in the LLCP scenario [46].

By increasing the resolution at intermediate T and exploring the metastable region of stretched water at $P < 0$, we find weak maxima in C_P at T below the liquid-to-gas spinodal line (Fig. 4b). For increasing $P < 0$ we find that the weak maxima occur at lower T and progressively merge into the strong maxima.

The origin of these maxima was studied by Mazza et al. [9] in the monolayer case. At any P the weak maximum at high temperature is produced by the energy fluctuations during the formation of new HBs, while the strong maxima at low temperature is produced by the effect of the cooperative reordering of the HB network. This interpretation agrees with our results for the evolution along isobars of N_{HB} and N_{coop} (Fig. 3). However the weak C_P maxima for the monolayer were observed also at $P > 0$ and were slowly increasing in intensity for increasing P before merging into the strong maxima [35], at variance with what we observe now for the bulk system.

Next, we calculate the thermal expansivity $\alpha_P \equiv (1/\langle V \rangle)(\partial\langle V \rangle / \partial T)_P$ along isobars and find extrema (minima) whose behavior is similar to those for C_P (Fig. 5). Specifically, we find strong minima at low T and weak minima at intermediate T that merge to the strong extrema for increasing P before reaching an apparent divergence for $Pv_0/(4\epsilon) = 0.85$, consistent with the behavior observed for C_P . The main difference with the results for C_P is that the strong extrema of α_P are

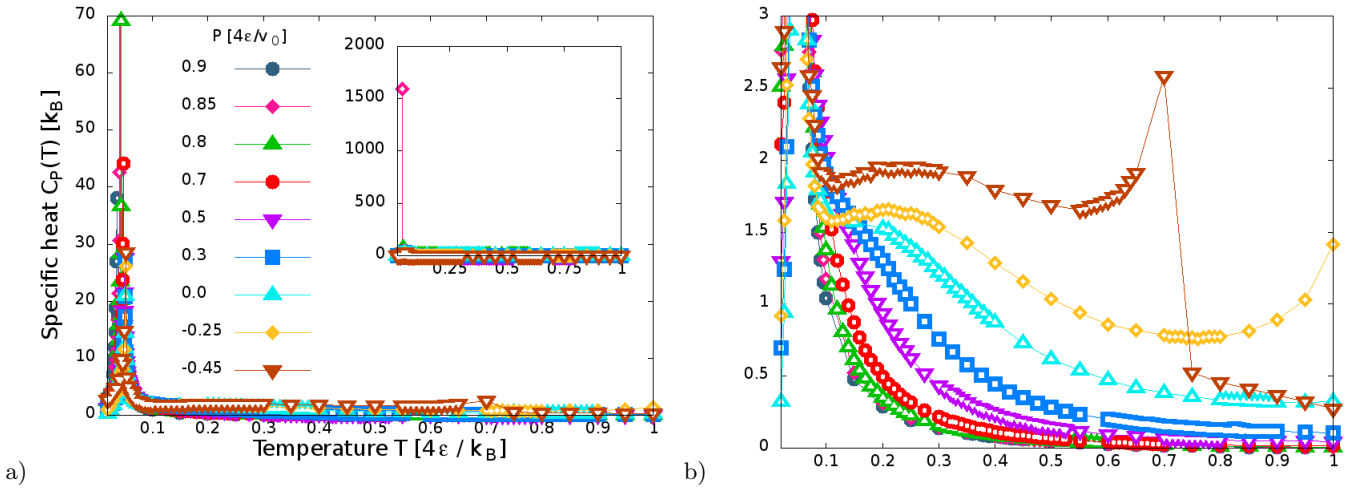


FIG. 4. Isobaric specific heat C_P calculated as function of T for different P . For sake of clarity we show only the results from the fluctuation-dissipation theorem. a) We find strong maxima at approximately constant T . The maxima increase for increasing $Pv_0/(4\epsilon) \leq 0.85$ with an apparent divergence at $Pv_0/(4\epsilon) = 0.85$ (inset). At higher P the maxima loose intensity and occur at lower T . b) By zooming into the values of C_P at intermediate T , we find also weak maxima at negative P . The weak maxima merge into the strong maxima as the pressure increases. The discontinuities found at $P < 0$ and high T are due to the crossing of the liquid-to-gas spinodal line.

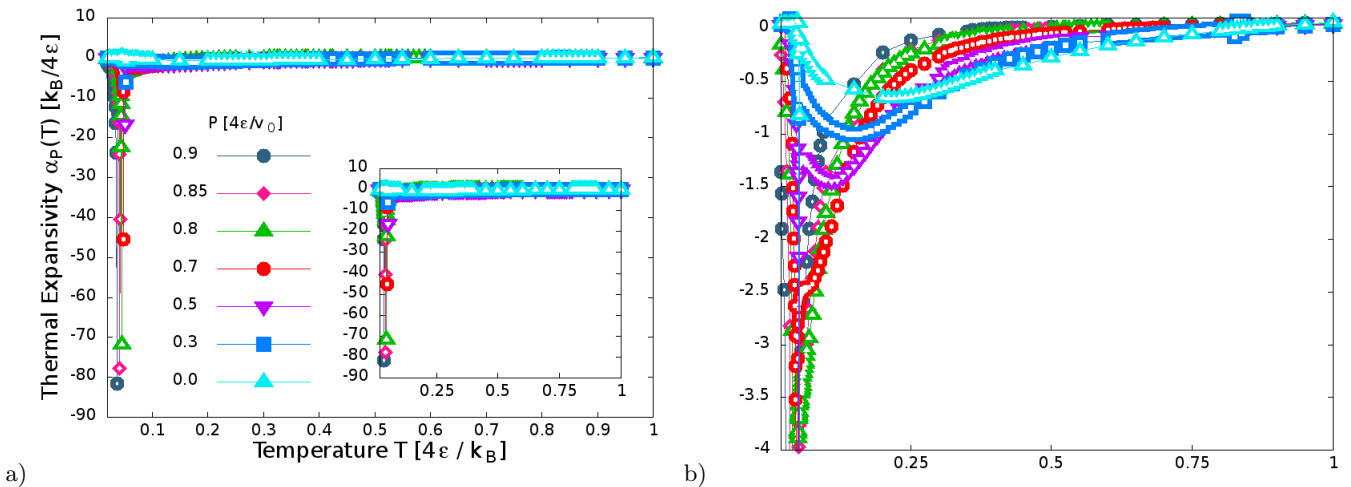


FIG. 5. Isobaric thermal expansivity α_P calculated as function of T . a) We find strong minima at low T for any $P > 0$. The minima occur at approximately constant T with an apparent divergence at $Pv_0/(4\epsilon) = 0.85$ (inset). At higher P the minima loose intensity and occur at lower T as for the maxima of C_P (Fig. 4). b) By zooming into the values of α_P at intermediate T , we find that the strong minima develop very sharp from weak minima at higher T . The weak minima merge into the strong minima as the pressure increases.

very sharp in T . However, both strong and weak extrema of α_P occur at approximately the same temperatures as those for C_P (Fig. 7). Furthermore, while the weak maxima of C_P are observable only for $P < 0$, the weak minima of α_P can be calculated for any $Pv_0/(4\epsilon) \leq 0.7$.

Finally, we calculate the isothermal compressibility K_T from the fluctuation-dissipation theorem, $K_T = \langle \Delta V^2 \rangle / k_B T V$, along isobars (Fig. 6). We find strong maxima for $0.7 < Pv_0/4\epsilon \leq 0.9$ with an apparent divergence at $Pv_0/(4\epsilon) = 0.85$ and weak maxima for $P > 0$.

The strong maxima are sharp as for the extrema of α_P . Furthermore we observe that the weak maxima of K_T occur at T higher than the weak extrema of α_P and that, approaching $P = 0$, they turn into minima. The minima occur at T increasing with $P > 0$.

In summary, the fluctuations of enthalpy associated to C_P , the fluctuations of volume associated to K_T and the cross fluctuations of volume and entropy associated to α_P increase when T decreases at constant P and display two maxima: a maximum occurring at a P -dependent

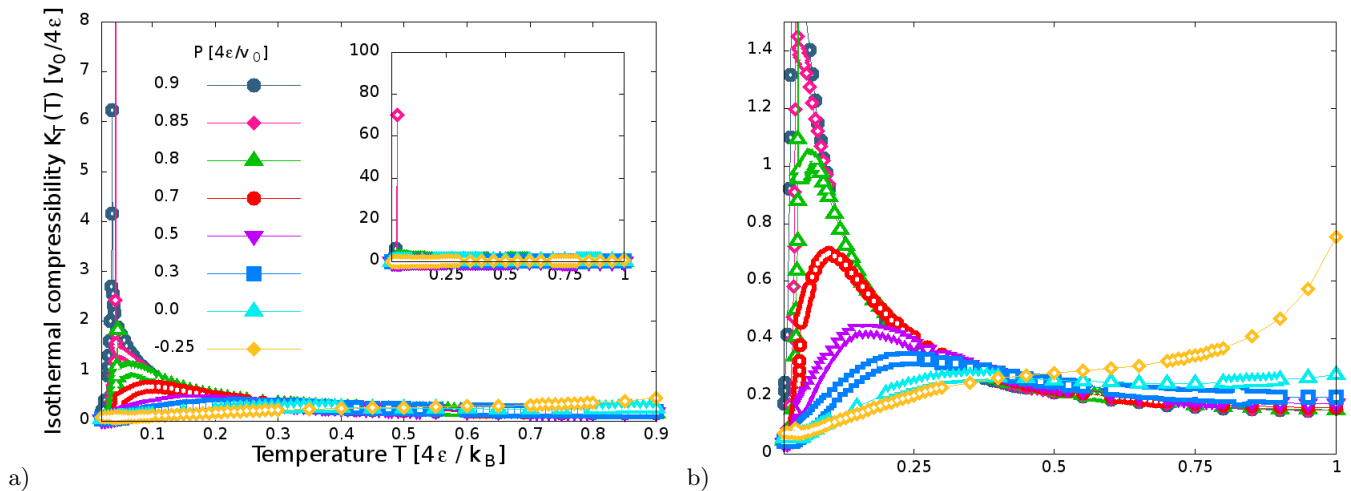


FIG. 6. Isothermal compressibility K_T calculated along isobars from the fluctuation-dissipation theorem. a) We find, at low T and any $P > 0$, maxima that smoothly grows and occur at lower T for higher P . b) A closer look at intermediate values $K_T(4\epsilon)/v_0 \simeq 1$ allows us to observe that, as for the case of α_P (Fig. 5), there are sharp extrema departing from the smooth (weak) extrema for $0.75 \leq P v_0/(4\epsilon) \leq 0.90$. The maxima occur all at approximately the same T and increase in intensity as P approaches $P v_0/(4\epsilon) = 0.85$ (inset in a). The weak maxima merge into the strong maxima at $P v_0/(4\epsilon) \simeq 0.85$. Finally, at high T and $0 \leq P v_0/(4\epsilon) \leq 0.2$, we find minima in K_T occurring at increasing T for increasing P .

value of T , and a strong maximum occurring a very low T that is almost P -independent.

The strong maxima appear at the same T where N_{coop} has the largest variation, i.e. where the fluctuations of N_{coop} are maxima. As a consequence, both the volume fluctuations for the Eq.(6), and the enthalpy fluctuation for the Eq.(7) are maxima near the same T [52]. Therefore, the strong maxima are due to the cooperative rearrangement of the HB network.

On the other hand, the weak maxima at higher temperatures are due to weak volume fluctuations associated to the formation of single HBs, coinciding with the largest variation of N_{HB} , as already seen for the water monolayer case [58, 59].

The resulting phase diagram (Fig. 7) of the 3D many-body water closely resemble the one observed for the monolayer case [35]. In the P - T phase diagram we find the liquid-to-gas (LG) spinodal at negative pressures defined as the point where K_T presents a huge increase and C_P has a discontinuous decrease due to the emergence of the gas phase. Above the LG spinodal we find a retracing TMD line that converges at low P toward the TminD line at low T , consistent with experimental data [60] and atomistic simulations [61]. Below the TMD line we find weak extrema at higher T and strong extrema at lower T for the response functions, $C_P(T)$, $K_T(T)$ and $\alpha_P(T)$. While the loci of weak extrema are P -dependent and merge at high P , the loci of strong extrema are P -independent and overlap. The locus of weak maxima of K_T converges at lower P toward the locus of minima of K_T as observed in atomistic simulations [61]. Furthermore, as can be demonstrated by thermodynamic argument [61], the locus of minima of K_T crosses the turning

point of the TMD line, showing that our results are thermodynamically consistent [35].

All the loci of strong and weak extrema converge toward the same high- P region where they all display a large increase near $P v_0/(4\epsilon) \simeq 0.85$ where they all seem to diverge. As demonstrated by finite size scaling for the case of a monolayer [35], this finding is consistent with the occurrence of a LLPT ending in a liquid-liquid critical point.

V. CONCLUSIONS

Our analysis shows that the bulk many-body water model reproduces the fluid properties of water in a wide range of pressures and temperatures. Below the liquid gas phase transition and above the liquid-to-gas spinodal in the stretched liquid state at $P < 0$, we find the TMD line and, at much lower T , the TminD line. The first at atmospheric pressure, corresponding to $P \simeq 0$ in our model, occurs at 277 K, while the second is estimated at a $T = 203 \pm 5$ K [62]. Therefore, the phase diagram we present here goes from the gas to the deep supercooled region of liquid water.

Below the TMD line, we find P -dependent extrema of the response functions C_P , α_P and K_T . While α_P has extrema at all the investigated P , C_P displays P -dependent maxima only at negative P , while K_T only at $P > 0$. In particular, the maxima of K_T converge toward minima for P approaching 0 and these minima cross the turning point of the TMD line as expected [61], showing that our results are thermodynamically consistent and similar to those of atomistic models for water [61, 63].

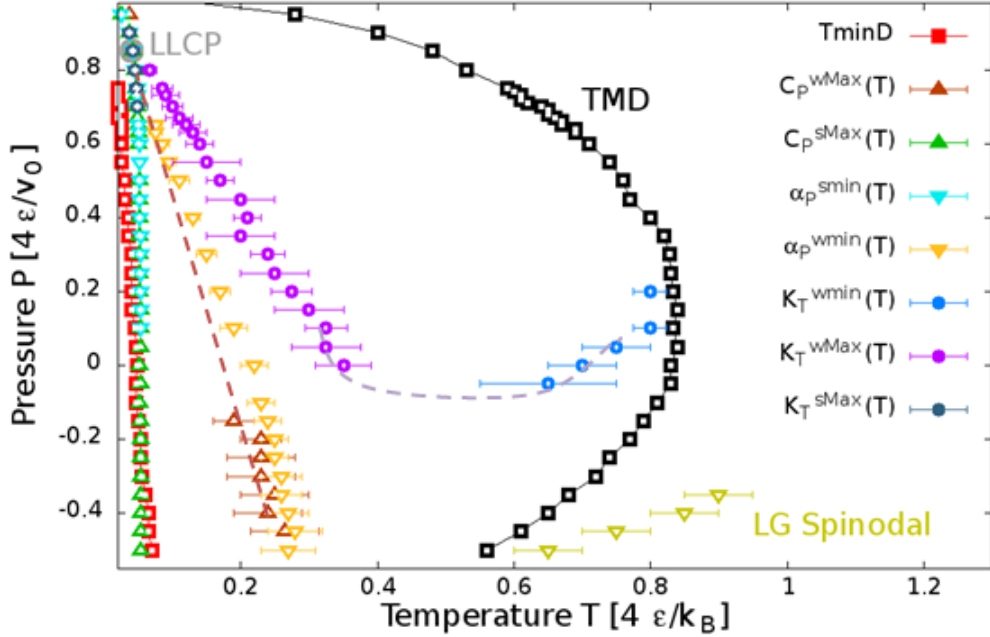


FIG. 7. The 3D many-body liquid water phase diagram in the P - T plane. Below the temperature of maximum density (TMD) line (black squares) and above the liquid-to-gas (LG) spinodal (green lower triangles) at low P and the temperature of minimum density (TminD) line (red squares), the loci of isobaric weak and strong extrema of, respectively, specific heat C_P^{wMax} (red upper triangles with dashed lines), C_P^{sMax} (green upper triangles), thermal expansivity α_P^{wmin} (yellow lower triangles), α_P^{smin} (turquoise lower triangles), and isothermal compressibility K_T^{wMax} (purple circles), K_T^{sMax} (green circles) cross all at $Pv_0/(4\epsilon) \simeq 0.85$, where we estimate the liquid-liquid critical point (LLCP, gray circle). The locus of K_T^{wMax} converges toward the locus of isobaric minima K_T^{wmin} (blue circles). Dashed lines are guides for the eyes.

However, our model allows us to simulate in an efficient way supercooled liquid water even at temperatures below the TminD line, an extremely demanding task for atomistic models as a consequence of the glassy slowing down of the dynamics [64, 65]. Thanks to this peculiar property we find that at $Tk_B/4\epsilon \simeq 0.035$, below the loci of the P -dependent maxima, all the response functions have sharp maxima that have almost no P dependence up to $Pv_0/(4\epsilon) \simeq 0.85$. We therefore call these maxima strong and call weak the P -dependent maxima. We find that the weak maxima merge with the strong maxima for $Pv_0/(4\epsilon) \leq 0.85$.

It is interesting to observe that weak and strong maxima have been found also in the monolayer many-body water model [35, 58, 59, 66] but with an important difference. For the monolayer case the strong maxima of C_P are observed also for $P > 0$, while for the bulk case they are overshadowed by the strong maxima at $P > 0$.

This difference between monolayer and bulk water is consistent with the fact that in the latter the total number of accessible states is much larger. In the case of the monolayer each molecule has four bonding variables with 6^4 accessible configurations [53]. Instead, for the bulk each molecule has six bonding variables with 6^6 accessible configurations. Therefore, the entropy loss due to the formation of the HB network is much greater for

the bulk with respect to the monolayer, consistent with a C_P with broader maxima that dominate over the weak maxima.

It is worth noticing that although our prediction of strong and weak maxima for the response functions has not been directly tested in atomistic models, it is perfectly consistent, qualitatively, with the results of atomistic simulations and at the same time with the experimental results [66]. Furthermore, several atomistic models give hints of more than one maxima in C_P , showing the line of P -dependent C_P maxima converging toward the line of C_P minima when crossing the point where the TMD line meets the TminD line [61, 63]. This convergence of loci of C_P maxima, TMD, TminD and C_P minima is consistent with the results for the water monolayer [35] and possibly also with the present results for bulk water.

We find that all the maxima of response functions merge and diverge at $Pv_0/(4\epsilon) \simeq 0.85$ and $Tk_B/4\epsilon \simeq 0.035$. Therefore we estimate the occurrence of a LLCP at these approximate values. A finite-size analysis, as the one performed for the monolayer case [35], would be necessary to estimate with larger confidence the LLCP. This analysis could also allow us to study the universality class of the LLCP in bulk. However, such analysis is beyond the scope of the present work.

For $Pv_0/(4\epsilon) > 0.85$ we find that the maxima of the response functions decrease and occur at lower T , consistent with a LLPT with negative slope in the P - T plane and ending in the LLCP, as found for the water monolayer [35].

In conclusion, our results for the bulk many-body water model are consistent with the LLCP scenario for supercooled liquid water [46]. Furthermore, we find properties consistent with those demonstrated in a rigorous way for the many-body water monolayer, including the occurrence of strong and weak maxima for the response functions [35]. Therefore, we can argue that these properties do not originate in the low-dimensionality of the monolayer system, but they are an intrinsic property of the model due to the cooperative contribution to the HB interactions. Because the cooperativity in water is a necessary implication of its peculiar properties [67, 68], we argue that our results are relevant for real water.

VI. ACKNOWLEDGMENTS

V.B. and G.F. acknowledge support from the Austrian Science Fund (FWF) project P 26253-N27 and the Spanish MINECO grant FIS2012-31025 and FIS2015-66879-C2-2-P, respectively.

Appendix A: Gas-liquid phase transition

We calculate isobars by applying an annealing protocol. We first simulate a random configuration at high temperature. Next we decrease the temperature and simulate starting from the equilibrated configuration of the previous step. Before reaching the liquid phase, water undergoes a gas-liquid phase transition (Fig. 8) with an abrupt increase of density in the transition from gas to liquid phase.

Appendix B: Error calculation in the specific heat

We made two independent calculations for the specific heat, one using the fluctuation-dissipation (FD) theorem and the other, using its definition as the temperature derivative of the enthalpy (TD). According to Statistical Physics, both results are equal under thermodynamic equilibrium conditions. For this reason, a good test to check whether the system is or is not equilibrated is to compare both results. If the system is well-equilibrated, they must overlap within their error bars.

We calculate average enthalpy $\langle H \rangle$ and fluctuations $\langle \Delta H^2 \rangle$ from the simulations and estimate the error using the Jackknife method. The method allows us also to estimate the MC correlation time as $\tau^{MC} \sim 256$ MC Steps. As a consequence we estimate that our averages are calculated over $\simeq 400$ independent simulations (Fig. 9).

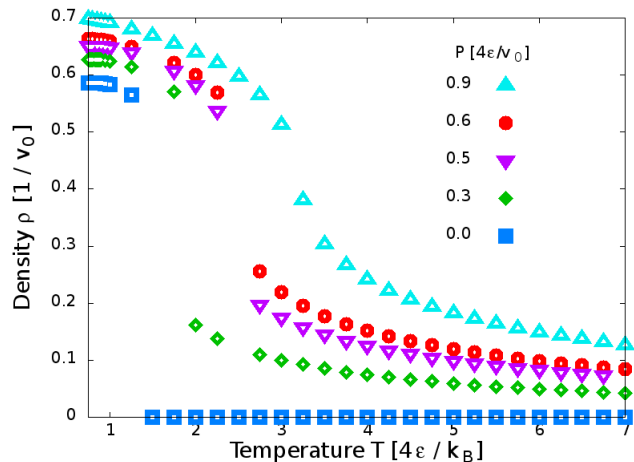


FIG. 8. Isobaric variation of the density at high temperatures. There is an abrupt change in the density as the system undergoes the gas-liquid phase transition

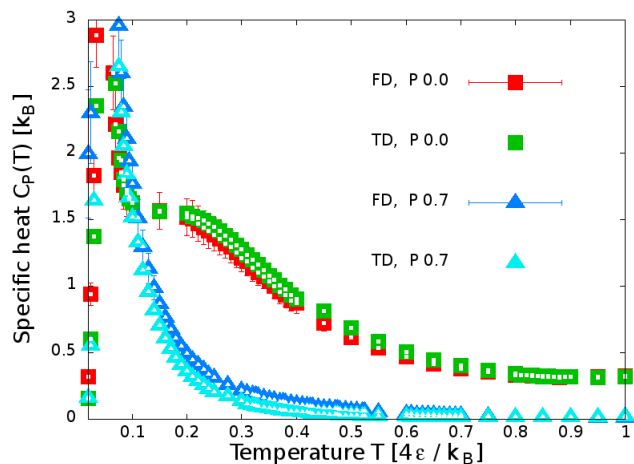


FIG. 9. Isobaric specific heat for two cases of high and low pressure. The resulting C_P obtained from TD fits within the errorbar of FD

On the one hand, the FD formula for the specific heat C_P and its error δC_P are

$$C_P^{FD} = \frac{\langle \Delta H^2 \rangle}{k_B T^2} \quad (B1)$$

$$\delta C_P^{FD} = \left| \frac{\partial C_P}{\partial \langle \Delta H^2 \rangle} \right| \delta \Delta H^2 = \frac{\delta \Delta H^2}{k_B T^2} \quad (B2)$$

On the other hand, the TD formula is

$$C_P^{TD} = \frac{\langle H(T) \rangle - \langle H(T - \Delta T) \rangle}{\Delta T} \quad (B3)$$

where we have used the numerical finite differences

method. The error for C_P in the TD method is

$$\delta C_P^{TD} = \frac{\delta\langle H(T) \rangle + \delta\langle H(T - \Delta T) \rangle}{\Delta T}. \quad (\text{B4})$$

-
- [1] Y. Levy and J. N. Onuchic, Proceedings of the National Academy of Sciences of the United States of America **101**, 3325 (2004).
- [2] G. Franzese, V. Bianco, and S. Iskvov, “Water at Interface with Proteins,” (2011).
- [3] V. Bianco, S. Iskvov, and G. Franzese, “Understanding the role of hydrogen bonds in water dynamics and protein stability,” (2012).
- [4] V. Bianco and G. Franzese, Phys. Rev. Lett. **115**, 108101 (2015).
- [5] B. J. Sirovets, N. P. Schafer, and P. G. Wolynes, J. Phys. Chem. B **119**, 11416 (2015).
- [6] F. Mallamace, C. Corsaro, D. Mallamace, S. Vasi, C. Vasi, P. Baglioni, S. V. Buldyrev, S.-H. Chen, and H. E. Stanley, Proceedings of the National Academy of Sciences of the United States of America **113**, 3159 (2016).
- [7] M. E. Johnson, C. Malardier-Jugroot, R. K. Murarka, and T. Head-Gordon, The Journal of Physical Chemistry B **113**, 4082 (2008).
- [8] K. L. Ngai, S. Capaccioli, and N. Shinyashiki, The Journal of Physical Chemistry B **112**, 3826 (2008).
- [9] M. Mazza and et al., Proc. Natl. Acad. Sci. USA **108** (2011).
- [10] G. Schirò and et al., Nat. Commun. **6** (2015).
- [11] A. Fogarty and D. Laage, The Journal of Physical Chemistry. B **118**, 7715 (2014).
- [12] F. Mallamace, C. Corsaro, D. Mallamace, N. Cicero, S. Vasi, G. Dugo, and H. E. Stanley, Frontiers of Physics **10**, 1 (2015).
- [13] M. Chaplin, Nature Rev. **7**, 861 (2006).
- [14] P. G. Debenedetti, *Metastable Liquids. Concepts and Principles* (Princeton University Press, Princeton, NJ, 1996).
- [15] J. R. Errington and P. G. Debenedetti, Nature **409**, 318 (2001).
- [16] C. Vega, J. L. F. Abascal, M. M. Conde, and J. L. Aragonés, Faraday Discuss **141**, 251 (2009).
- [17] P. Barnes and et al., Nature **282** (1979).
- [18] J. D. Cruzan and et al., Science **271**, 59 (1996).
- [19] C. Perez and et al., Angew. Chem. **53**, 14596 (2014).
- [20] J. M. Guevara-Vela and et al., Phys. Chem. Chem. Phys. (2016).
- [21] A. L. Agapov and et al., Phys. Rev. E **91**, 022312 (2015).
- [22] H. Kanno and C. A. Angell, The Journal of Chemical Physics **70**, 4008 (1979).
- [23] C. A. Angell, W. J. Sichina, and M. Oguni, Journal of Physical Chemistry **86**, 998 (1982).
- [24] P. H. Poole, F. Sciortino, T. Grande, H. E. Stanley, and C. A. Angell, Physical Review Letters **73**, 1632 (1994).
- [25] H. Tanaka, Nature **380**, 328 (1996).
- [26] O. Mishima and H. E. Stanley, **392**, 164 (1998).
- [27] A. K. Soper and M. A. Ricci, Physical Review Letters **84**, 2881 (2000).
- [28] W.-X. Xu, J. Wang, and W. Wang, Proteins-Structure Function And Genetics **61**, 777 (2005).
- [29] D. Liu, Y. Zhang, C.-C. Chen, C.-Y. Mou, P. H. Poole, and S.-H. Chen, Proceedings of the National Academy of Sciences **104**, 9570 (2007).
- [30] K. Stokely, M. G. Mazza, H. E. Stanley, and G. Franzese, Proceedings of the National Academy of Sciences of the United States of America **107**, 1301 (2010).
- [31] J. L. F. Abascal and C. Vega, The Journal of Chemical Physics **133**, 234502 (2010).
- [32] C. E. Bertrand and M. A. Anisimov, The Journal of Physical Chemistry B **115**, 14099 (2011).
- [33] V. Holten, D. T. Limmer, V. Molinero, and M. A. Anisimov, The Journal of Chemical Physics **138**, 174501 (2013).
- [34] G. Pallares, M. El Mekki Azouzi, M. A. González, J. L. Aragonés, J. L. F. Abascal, C. Valeriani, and F. Caupin, Proceedings of the National Academy of Sciences **111**, 7936 (2014), <http://www.pnas.org/content/111/22/7936.full.pdf>.
- [35] V. Bianco and G. Franzese, Scientific Reports **4**, 4440 (2014).
- [36] A. K. Soper, Nature materials **13**, 671 (2014).
- [37] A. Nilsson and L. G. M. Pettersson, Nature communications **6**, 8998 (2015).
- [38] F. Sciortino, I. Saika-Voivod, and P. H. Poole, Phys. Chem. Chem. Phys. **13**, 19759 (2011).
- [39] Y. Liu, J. C. Palmer, A. Z. Panagiotopoulos, and P. G. Debenedetti, The Journal of Chemical Physics **137**, 214505 (2012).
- [40] J. C. Palmer, R. Car, and P. G. Debenedetti, Faraday Discuss. **167**, 77 (2013).
- [41] P. H. Poole, R. K. Bowles, I. Saika-Voivod, and F. Sciortino, The Journal of Chemical Physics **138**, 34505 (2013).
- [42] J. C. Palmer, F. Martelli, Y. Liu, R. Car, A. Z. Panagiotopoulos, and P. G. Debenedetti, Nature **510**, 385 (2014).
- [43] F. Smallenburg and F. Sciortino, Physical review letters **115**, 015701 (2015).
- [44] R. J. Speedy, The Journal of Physical Chemistry **86**, 982 (1982).
- [45] S. Sastry, P. G. Debenedetti, F. Sciortino, and H. E. Stanley, Physical Review E **53**, 6144 (1996).
- [46] P. Poole, F. Sciortino, U. Essmann, and H. Stanley, Nature **360**, 324 (1992).
- [47] C. A. Angell, Science **319**, 582 (2008).
- [48] D. A. Fuentesvilla and M. A. Anisimov, Phys. Rev. Lett. **97**, 195702 (2006).
- [49] G. Franzese, M. I. Marqués, and H. E. Stanley, Physical Review E **67**, 11103 (2003).
- [50] G. Franzese and H. Stanley, J. Phys. Condes. Matter **14**, 2201 (2002).
- [51] G. Franzese and H. Stanley, J. Phys.: Condes. Matter **19** (2007).
- [52] G. Franzese and H. E. Stanley, Journal of Physics: Con-

- densed Matter **19**, 205126 (2007).
- [53] F. de los Santos and G. Franzese, The Journal of Physical Chemistry B (2011), 10.1021/jp206197t.
- [54] O. Vilanova and G. Franzese, arXiv:1102.2864 (2011).
- [55] We adopt two-axis periodic boundary conditions in such a way to be able to perform consistent checks with previous results for the monolayer model.
- [56] M. G. Mazza, K. Stokely, E. G. Strelakova, H. E. Stanley, and G. Franzese, *Special issue based on the Conference on Computational Physics 2008 - CCP 2008*, Computer Physics Communications **180**, 497 (2009).
- [57] H. E. Stanley and J. Teixeira, The Journal of Chemical Physics **73**, 3404 (1980).
- [58] M. G. Mazza, K. Stokely, S. E. Pagnotta, F. Bruni, H. E. Stanley, and G. Franzese, Proceedings of the National Academy of Sciences **108**, 19873 (2011).
- [59] M. G. Mazza, K. Stokely, H. E. Stanley, and G. Franzese, The Journal of Chemical Physics **137**, 204502 (2012).
- [60] F. Mallamace and et al., Proc Natl Acad Sci USA **104**, 18387 (2007).
- [61] P. H. Poole, I. Saika-Voivod, and F. Sciortino, J. Phys.: Condens. Matter **17**, L431 (2005).
- [62] F. Mallamace, C. Branca, M. Broccio, C. Corsaro, C.-Y. Mou, and S.-H. Chen, Proceedings of the National Academy of Sciences of the United States of America **104**, 18387 (2007).
- [63] M. A. González, C. Valeriani, F. Caupin, and J. L. F. Abascal, The Journal of Chemical Physics **145**, 054505 (2016), <http://dx.doi.org/10.1063/1.4960185>.
- [64] T. Kesselring, G. Franzese, S. Buldyrev, H. Herrmann, and H. E. Stanley, Nature Scientific Reports **2**, 474 (2012).
- [65] T. Kesselring, E. Lascaris, G. Franzese, S. V. Buldyrev, H. Herrmann, and H. E. Stanley, Journal of Physical Chemistry **138**, 244506 (2013), arXiv:1302.1894 [cond-mat.soft].
- [66] V. Bianco, M. G. Mazza, K. Stokely, , F. Bruni, H. E. Stanley, and G. Franzese, in *Proceedings of "Symposium on the Fragility of Glass-formers: A Conference in Honor of C. Austen Angell"*, edited by R. Ganapathy, A. L. Greer, K. F. Kelton, and S. Sastry (2013).
- [67] P. Barnes, J. L. Finney, J. D. Nicholas, and J. E. Quinn, Nature **282**, 459 (1979).
- [68] J. M. Guevara-Vela, E. Romero-Montalvo, V. A. Mora-Gomez, R. Chavez-Calvillo, M. Garcia-Revilla, E. Francisco, A. Martin Pendas, and T. Rocha-Rinza, Physical Chemistry Chemical Physics (2016), 10.1039/C6CP00763E.